ELECTRONIC SUPPLEMENTARY INFORMATION

FOR

Imposing high-symmetry and tuneable geometry on lanthanide centres with chelating Pt and Pd metalloligands

Mikkel A. Sørensen, Høgni Weihe, Morten G. Vinum, Jesper S. Mortensen, Linda H. Doerrer and Jesper Bendix*

Chemical Science

CONTENTS

Syntheses

KSAc (Sigma-Aldrich *or* Acros Organics, > 98 %), $K_2[PtCl_4]$ (Pressure Chemicals), $Na_2[PdCl_4]$ (Pressure Chemicals), $LaCl_3{\cdot}7H_2O$ (Merck), $CeCl_3{\cdot}7H_2O$ (Sigma-Aldrich, 99.9 %), $PrCl_3{\cdot}xH_2O$ (Sigma-Aldrich, 99.9 %), $NdCl_3{\cdot}6H_2O$ (Sigma-Aldrich, 99.9 %), $SmCl_3{\cdot}6H_2O$ (Sigma-Aldrich, ≥ 99 %), $GdCl_3{\cdot}6H_2O$ (Sigma-Aldrich, 99 %), $TbCl_3{\cdot}6H_2O$ (Sigma-Aldrich, 99.9 %), $HoCl_3{\cdot}6H_2O$ (Sigma-Aldrich, 99.9 %), $ErCl_3{\cdot}6H_2O$ (Sigma-Aldrich, 99.9 %), $TmCl_3$ (Sigma-Aldrich, 99.9 %), $YbCl_3{\cdot}6H_2O$ (Sigma-Aldrich, 99.9 %), $LuCl_3{\cdot}6H_2O$ (Acros Organics, 99.90 %), $[NEt_4]Cl{\cdot}xH_2O$ (Acros Organics, 99 %), $[N^nPr_4]Br$ (Sigma-Aldrich, 98 %), $[PPh_4]Cl$ (chemPUR, 98+ %), $MeNO_2$ (Carl Roth, ≥ 97 %), Et_2O (VWR Prolabo Chemicals, < 1 g H_2O/l), and acetone (technical) were bought from commercial suppliers and used as received. $EuCl_3{\cdot}6H_2O$ was prepared from the corresponding oxide (99.99 %, Stanford Materials Corporation) by refluxing excess oxide in hydrochloric acid (Sigma-Aldrich, ≥ 37 % HCl) diluted with water. Filtering off the undissolved oxide and evaporating the solvent at reduced pressure gave the hydrated chloride as a white crystalline solid. Elemental analyses were performed by the microanalytical services of the Department of Chemistry, University of Copenhagen.

$[NEt_4][Ln\{Pt(SAc)_4\}_2]$ (1Ln) (Ln = La – Nd, Sm – Ho, Y): KSAc (171 mg, 1.50 mmol) was dissolved in water (La, 120 ml; Ce, 90 ml; Pr, 70 ml; Nd, 60 ml; Sm, 45 ml; Eu, 30 ml; Gd, 21 ml; Tb, 18 ml; Dy, 12 ml; Ho, 3.0 ml; Y, 3.0 ml) with stirring and a solution of $K_2[PtCl_4]$ (155 mg, 0.374 mmol) in water (4.5 ml) was added. The reddish solution was added a solution of $LnCl_3{\cdot}xH_2O$ (0.188 mmol) dissolved in water (3.0 ml). After stirring for 2 hours at ambient temperature the color of the solution had changed towards light golden-yellow. The solution was filtered and added a solution of $[NEt_4]Cl{\cdot}xH_2O$ (90 mg, 0.54 mmol for $x = 0$) in water (1.5 ml). Within minutes, golden-yellow square-shaped crystals started to appear (the crystals of **1Ho** are either glimmering pink or golden-yellow depending on the light source). The reaction mixture was left for crystallization at 5 °C overnight. The crystals were isolated by filtration, washed with water (2 × 30 ml), acetone (30 ml), and dried in air. Yields are 40–75 % based on the amount of employed lanthanide chloride. Anal. calcd. (found) for $C_{24}H_{44}LnNO_8Pt_2S_8$ (**1Ln**): **1La**, C, 22.87 (23.07); H, 3.52 (3.50); N, 1.11 (1.12); S, 20.36 (20.50). **1Ce**, C, 22.85 (22.60); H, 3.52 (3.52); N, 1.11 (1.13); S, 20.3 (20.8). **1Pr**, C, 22.84 (22.99); H, 3.51 (3.47); N, 1.11 (1.07); S, 20.32 (20.11). **1Nd**, C, 22.78 (22.97); H, 3.50 (3.48); N, 1.11 (1.09); S, 20.27 (20.12). **1Sm**, C, 22.67 (22.91); H, 3.49 (3.46); N, 1.10 (1.07); S, 20.17 (20.12). **1Eu**, C, 22.64 (22.86); H, 3.48 (3.44); N, 1.10 (1.08); S, 20.15 (19.91). **1Gd**, C, 22.55 (22.57); H, 3.47 (3.42); N, 1.10 (1.10); S, 20.06 (20.07). **1Tb**, C, 22.52 (22.68); H, 3.46 (3.42); N, 1.09 (1.10); S, 20.04 (20.17). **1Dy**, C, 22.45 (22.66); H, 3.45 (3.42); N, 1.09 (1.08); S, 19.98 (19.98). **1Ho**, C, 22.41 (22.55); H, 3.45 (3.44); N, 1.09 (1.10); S, 19.94 (20.10). **1Y**, C, 23.82 (23.90); H, 3.66 (3.68); N, 1.16 (1.13); S, 21.20 (21.42).

$[NEt_4][Ln\{Pt(SAc)_4\}_2]$ (1Ln) (Ln = Er – Yb): KSAc (165 mg, 1.44 mmol) and $K_2[PtCl_4]$ (150 mg, 0.361 mmol) were dissolved together in water (Er, 6.0 ml; Tm, 5.0 ml; Yb; 4.0 ml). The reddish solution was heated over a moderate Bunsen burner flame for 30–40 s resulting in a color change to light yellow, and subsequently cooled until lukewarm. The solution was filtered, and added solid $LnCl_3{\cdot}xH_2O$ (0.18 mmol). After dissolution of the chloride a slight turbidity developed, the turbidity being the most pronounced for Yb and the least for Er. $[NEt_4]Cl{\cdot}xH_2O$ (700 mg, 4.22 mmol for $x = 0$) dissolved in water (1.0 ml) was added to the reaction mixture, causing the turbidity to disappear completely. Heating the clear solution to a boil over a moderate Bunsen burner flame resulted in the crystallization of golden-yellow square-shaped crystals. Occasionally, the crystals appear orange due to surface effects. The reaction mixture was left at 5 °C overnight for completion of the crystallization. The crystals were isolated be filtration, washed with water (2 × 20 ml), acetone (20 ml), and dried in air. Yields are 40–60 % based on the amount of employed lanthanide chloride. Anal. calcd. (found) for $C_{24}H_{44}LnNO_8Pt_2S_8$ (**1Ln**): **1Er**, C, 22.37 (22.35); H, 3.44 (3.44); N, 1.09 (1.08); S, 19.91 (19.88). **1Tm**, C, 22.34 (22.23); H, 3.44 (3.42); N, 1.09 (1.07); S, 19.88 (19.83). **1Yb**, C, 22.28 (22.36); H, 3.43 (3.40); N, 1.08 (1.07); S, 19.82 (19.89).

[NEt$_4$][Lu{Pt(SAc)$_4$}$_2$] (1Lu): KSAc (165 mg, 1.44 mmol) and $K_2[PtCl_4]$ (150 mg, 0.361 mmol) were dissolved in water (3.0 ml), and the resulting reddish solution was heated over a moderate Bunsen burner flame for 30–40 s resulting in a color change to light yellow. The solution was subsequently cooled until lukewarm, filtered, and added solid $LuCl_3 \cdot 6H_2O$ (70 mg, 0.18 mmol), causing the formation of a significant amount of precipitate. Addition of a solution of $[NEt_4]Cl \cdot xH_2O$ (700 mg, 4.22 mmol for $x = 0$) in water (1.0 ml) to the reaction mixture caused most of the precipitate to redissolve. The slightly turbid yellow solution was filtered, and heated to a boil over a moderate Bunsen burner flame which resulted in the crystallization of golden-yellow square-shaped crystals. The reaction mixture was left at 5 °C overnight for completion of the crystallization. The crystals were isolated be filtration, washed with water (2 × 20 ml), acetone (20 ml), and dried in air. As evidenced by Powder X-ray Diffraction (PXRD) the sample is contaminated by a small amount of an unknown crystalline impurity. The yield is 10-20 % based on the amount of lutetium chloride used. Anal. calcd. (found) for $C_{24}H_{44}LuNO_8Pt_2S_8$ (**1Lu)**: C, 22.24 (21.99); H, 3.42 (3.34); N, 1.08 (1.02); S, 19.79 (20.16).

[N^{n}Pr$_4$][Ln{Pt(SAc)$_4$}$_2$] (Ln = Gd – Er, Y): KSAc (165 mg, 1.44 mmol) and $K_2[PtCl_4]$ (150 mg, 0.361 mmol) were dissolved together in water (Gd, 10 ml; Tb, 7.0 ml; Dy, 6.0 ml; Ho; 6.0 ml; Er, 6.0 ml, Y; 6.0 ml). Heating the solution over a moderate Bunsen burner flame for 30–40 s resulted in a color change to light yellow. The resulting solution was allowed to cool until lukewarm, filtered, and added solid $LnCl_3 \cdot xH_2O$ (0.18 mmol). When the chloride had dissolved, [N^{n}Pr$_4$]Br (1.13 g, 4.24 mmol) dissolved in water (Gd, 3.0 ml; Tb, 3.0 ml; Dy, 2.5 ml; Ho, 2.0 ml; Er, 0 ml (the solid bromide salt was added); Y, 2.0 ml) was added to the reaction mixture. Heating the solution to a boil over a moderate Bunsen burner flame resulted in the precipitation of a yellow to orange powder. After standing at 5 °C overnight, the product was isolated by filtration. The powder was washed with Et_2O (20 ml) and air-dried. Yields are 40–80 % based on the amount of employed lanthanide chloride. The compounds can be crystallized by slow evaporation of a filtered solution of the powders in acetone (10 mg/ml). Anal. calcd. (found) for $C_{28}H_{52}LnNO_8Pt_2S_8$ ([N^{n}Pr$_4$][Ln{Pt(SAc)$_4$}$_2$]): Gd, C, 25.20 (25.33); H, 3.93 (3.88); N, 1.05 (1.04); S, 19.22 (19.13). Tb, C, 25.17 (25.40); H, 3.92 (3.87); N, 1.05 (1.03); S, 19.20 (19.25). Dy, C, 25.10 (25.28); H, 3.91 (3.89); N, 1.05 (1.00); S, 19.14 (19.24). Ho, C, 25.05 (25.15); H, 3.90 (3.85); N, 1.04 (0.98); S, 19.11 (19.19). Er, C, 25.01 (25.18); H, 3.90 (3.89); N, 1.04 (1.00); S, 19.1 (19.8). Y, C, 26.56 (26.65); H, 4.14 (4.06); N, 1.11 (1.06); S, 20.26 (20.23). Upon recrystallization, the solubility of the salts drops significantly. As a result, the crude [N^{n}Pr$_4$][Ln{Pt(SAc)$_4$}$_2$] salts are best suited for the synthesis of **2Ln** following the procedure described below.

[PPh$_4$][Ln{Pt(SAc)$_4$}$_2$] (2Ln) (Ln = Gd – Er, Y): To a filtered solution of crude [N^{n}Pr$_4$][Ln{Pt(SAc)$_4$}$_2$] (0.100 mmol) in $MeNO_2$ (15 ml) was added a solution of [PPh$_4$]Cl (37 mg, 0.10 mmol) in $MeNO_2$ (2 ml). Immediately, crystallization of **2Ln** commenced. The product was allowed to precipitate for approximately 15 minutes. Recrystallization was achieved by heating the suspension to a boil and allowing the resulting clear solution to stand overnight at 5 °C. The golden-yellow, square-shaped crystals of **2Ln** were isolated by filtration, washed with acetone (15 ml), and dried in air. Yields are 70–75 % based on [N^{n}Pr$_4$][Ln{Pt(SAc)$_4$}$_2$]. Anal. calcd. (found) for $C_{40}H_{44}LnO_8PPt_2S_8$ (**2Ln**): **2Gd**, C, 32.29 (32.40); H, 2.98 (2.92); S, 17.24 (17.38). **2Tb**, C, 32.26 (32.25); H, 2.98 (2.89); S, 17.22 (17.04). **2Dy**, C, 32.18 (32.20); H, 2.97 (2.94); S, 17.18 (17.14). **2Ho**, C, 32.13 (32.22); H, 2.97 (2.91); S, 17.15 (17.04). **2Er**, C, 32.08 (31.98); H, 3.12 (3.08); S, 17.13 (17.36). **2Y**, C, 33.85 (33.83); H, 3.12 (3.08); S, 18.07 (18.14). Crystals of **2Ln** tend to suffer from significant intergrowth. Crystals suited for single crystal X-ray diffraction experiments were obtained by downscaling the above procedure, starting from 10 mg of the crude [N^{n}Pr$_4$][Ln{Pt(SAc)$_4$}$_2$] salts.

[NEt$_4$][Y{Pd(SAc)$_4$}$_2$] (1Y′): KSAc (542 mg, 4.73 mmol) was dissolved in water (2.5 ml). To this, a filtered solution of $Na_2[PdCl_4]$ (316 mg, 1.07 mmol) in water (6 ml) was added slowly, dropwise, ensuring complete conversion between each successive addition. To the resulting solution was added $YCl_3 \cdot 6H_2O$ (164 mg, 0.541 mmol) dissolved in water (1.5 ml). The reaction mixture was filtered and added, with stirring, a solution of $[NEt_4]Cl \cdot xH_2O$ (1.60 g, 9.66 mmol for $x = 0$) dissolved in water (2.5 ml). The reaction mixture was left stirring for 5 min. and subsequently cooled to 5°C. The bright yellow, microcrystalline product was collected by filtration and washed with water twice and once with acetone. Yield. 348 mg (63%) based on $YCl_3 \cdot 6H_2O$. Anal. calcd. (found) for $C_{24}H_{44}YNO_8Pd_2S_8$ (**1Y′**): C, 27.91 (27.58); H, 4.29 (4.33); N, 1.36 (1.43); S, 24.84 (24.80). Single crystals suitable for single crystal X-ray diffraction were obtained by leaving the reaction mixture undisturbed at 5°C subsequent to the addition of the $[NEt_4]Cl \cdot xH_2O$ solution.

[NEt$_4$][Gd{Pd(SAc)$_4$}$_2$] (1Gd′): KSAc (548 mg, 4.80 mmol) was dissolved in water (8.5 ml). To this a filtered solution of $Na_2[PdCl_4]$ (319 mg, 1.08 mmol) in water (10 ml) was added slowly, dropwise, ensuring complete conversion between each successive addition. The resulting pale yellow solution was allowed to stir for 5 min, and then added $GdCl_3 \cdot 6H_2O$ (208 mg, 0.560 mmol) dissolved in water (1.3 ml). The slightly turbid reaction mixture was filtered and added, with stirring, a solution of $[NEt_4]Cl \cdot xH_2O$ (1.59 g, 9.60 mmol for $x = 0$) dissolved in water (2.0 ml). The reaction mixture was left stirring for 5 min. and subsequently cooled to 5°C. The bright yellow, microcrystalline product was collected by filtration and washed with water twice and once with acetone. Yield. 392 mg (66%) based on $GdCl_3 \cdot 6H_2O$. Anal. calcd. (found) for $C_{24}H_{44}GdNO_8Pd_2S_8$ (**1Gd′**): C, 26.18 (26.06); H, 4.03 (4.18); N, 1.27 (1.40); S, 23.29 (23.34). Single crystals suitable for single crystal X-ray diffraction were obtained by leaving the reaction mixture undisturbed at 5°C subsequent to the addition of the $[NEt_4]Cl \cdot xH_2O$ solution.

[N^{n}Pr$_4$][Ln{Pd(SAc)$_4$}$_2$] (Ln = Y, Gd): KSAc (Y, 543 mg, 4.73 mmol; Gd, 410 mg, 3.59 mmol) was dissolved in water (Y, 2.0 ml; Gd, 3.0 ml). To this a filtered solution of $Na_2[PdCl_4]$ (Y, 321 mg, 1.09 mmol; Gd, 240 mg, 0.816 mmol) in water (Y, 7 ml; Gd, 12 ml) was added slowly, dropwise, ensuring complete conversion between each successive addition. The resulting yellow solution was allowed to stir for 5 min. Solid $LnCl_3 \cdot 6H_2O$ (Y, 164 mg, 0.541 mol; Gd, 150 mg, 0.404 mmol) was added. After 5 min of stirring the solution was filtered. The solution was added a solution of [N^{n}Pr$_4$]Br in water (Y, 3.40 g, 12.8 mmol; Gd, 2.70 g, 10.1 mmol). The reaction mixture was stirred vigorously for 10 min yielding a pale yellow product. The product was isolated by filtration and washed with water and Et_2O (2 × 4 ml). Yield: Gd, 354 mg (76 %); Y, 375 mg (64 %) based on the employed amount of $LnCl_3 \cdot 6H_2O$. Anal. calcd. (found) for $C_{28}H_{52}LnNO_8Pd_2S_8$ ([N^{n}Pr$_4$][Ln{Pd(SAc)$_4$}$_2$]): Y, C, 30.88 (31.00); H, 4.81 (4.82); N, 1.29 (1.25); S, 23.56 (23.56); Gd, C, 29.06 (29.25); H, 4.53 (4.52); N, 1.21 (1.16); S, 22.16 (22.06).

[PPh$_4$][Ln{Pd(SAc)$_4$}$_2$] (2Ln′) (Ln = Y, Gd): To a filtered solution of crude [N^{n}Pr$_4$][Ln{Pd(SAc)$_4$}$_2$] (Y, 170 mg, 0.156 mmol; Gd, 151 mg, 0.131 mmol) in $MeNO_2$ (19 ml) was added a solution of [PPh$_4$]Cl (Y, 60 mg, 0.16 mmol; Gd, 49 mg, 0.13 mmol) in $MeNO_2$ (2.5 ml). From the stirred reaction mixture crystallization commences. The solution is heated gently to dissolve the initial precipitate and left at 5°C for crystallization. The yellow crystalline product was isolated by filtration and washed with acetone. Yield: Y, 115 mg (59%); Gd, 104 mg (61%) based on [N^{n}Pr$_4$][Ln{Pd(SAc)$_4$}$_2$]. Anal. calcd. (found) for $C_{40}H_{44}LnO_8PPd_2S_8$ (**2Ln′**): **2Y′**, C, 38.68 (38.78); H, 3.57 (3.55); S, 20.65 (20.79). **2Gd′**, C, 36.66 (36.78); H, 3.38 (3.32); S, 19.58 (19.29).

X-Ray diffraction

Single-crystal X-ray diffraction data were collected on a Bruker D8 VENTURE diffractometer equipped with Mo Kα high brilliance IμS radiation (λ = 0.71073 Å), a multilayer X-ray mirror a PHOTON 100 CMOS detector, and an Oxford Cryosystems low temperature device. Crystals were mounted on loops made of Kapton. If deemed necessary, crystals were covered in mineral oil prior to mounting. The diffractometer was controlled using the SAINT program[1] as implemented in the APEX2 software package. Intensity data were corrected for absorption using the multi-scan method implemented in SADABS.[2] The structures were solved using Olex2[3] by means of the olex2.structure solution program[3] using a quasi-*E* charge flipping algorithm and refined with the olex2.refine refinement package[4] using Gauss-Newton minimization. All non-hydrogen atoms were refined anisotropically and all hydrogens but those of the tetraethylammonium ions of **1Ln** and **1Ln′** were placed at calculated positions and refined with isotropic displacement parameters using a riding model. For all **1Ln** and **1Ln′** structures, the hydrogen atoms of the tetraethylammonium cation were impossible to place at calculated positions as a result of the disorder induced by the location of the nitrogen atom on a special position with fractional coordinates (0,0,½) and site symmetry 4/*m*… The methylene carbon hydrogen atoms were localized in the Fourier map as a single *Q*-peak. This position corresponds to the average position of two half-occupied hydrogen atoms bound to neighbouring disordered methylene groups. Three *Q*-peaks could be located close to the methyl group carbon atom. These were assigned to hydrogen atoms, and the C–H bond distance restrained to 0.96(2) Å using the DFIX command, resulting in a total of three restraints. The occupancies were given values that resulted in approximately equal isotropic displacement parameters and a sum of 1.5, in order to arrive at three hydrogen atoms per methyl group. Two of the hydrogen atoms reside on special positions with site symmetry *m*.., while the third occupies a general position. This results in four positions for the hydrogen atoms belonging to the methyl group. The limited physical meaningfulness of this reflects the ill-defined positions of the three atoms resulting from the symmetry-induced disorder of the cation. In the structures of **1Ln** and **1Ln′**, the thioacetate contained in the asymmetric unit experiences static disorder over two positions with

a 50:50 occupancy ratio. The fragments have separate positions of the oxygen and sulphur atoms, but share the $–CCH_3$ moiety. As a result of this disorder, the site symmetry is arguably lower (C_4) than that otherwise inferred from the crystallographic analysis (D_4). Consequently, the appropriate description of the magnetic/electronic properties assumes a single lanthanide site of C_4 symmetry. For **2Ln** and **2Ln′**, the room temperature structure determinations indicate the introduction of a very slight disorder in the thioacetate similar to that observed for the **1Ln** and **1Ln′** structures. The disorder is however too small to be reliably refined, indicating that it is of a dynamic nature. Powder X-ray diffraction data were collected at room temperature on a Bruker D8 ADVANCE powder diffractometer operating in a 2θ-θ configuration using Cu Kα radiation (λ = 1.5418 Å). The samples were ground in an agate mortar, and adhered onto a quadratic piece of double sided Kapton tape fastened on a poly(methyl methacrylate) sample holder. This particular sample holder gives rise to a slight curvature in the low-angle background. The simulated powder patterns were calculated from the relevant .cif files using the Mercury 3.7 software[5] including $K\alpha_1$ as well as $K\alpha_2$. The inherently plate-shaped nature of the crystals results in pronounced orientation effects in the experimental powder patterns, despite the samples being thoroughly ground prior to the diffraction experiments. These effects are most dominant in the powder patterns for the **1Ln** and **1Ln′** salts, where the (0 0 *l*) reflections with $l = 2n$ have remarkably increased intensities. This is especially true for the (0 0 4) Bragg peak which occasionally appears equally or even more intense than the (1 0 0) peak, which is otherwise the most intense in the case of perfect powder averaging.

Table S1. Crystallographic data and refinement parameters for **1Ln** (**Ln = La – Nd**).

	1La	**1Ce**	**1Pr**	**1Nd**
Formula	$C_{24}H_{44}LaNO_8Pt_2S_8$	$C_{24}H_{44}CeNO_8Pt_2S_8$	$C_{24}H_{44}NO_8PrPt_2S_8$	$C_{24}H_{44}NNdO_8Pt_2S_8$
M_r	1260.21	1261.42	1262.21	1265.54
T / K	122(1)			
Crystal system	Tetragonal			
Space group	*P*4/*mcc* (No. 124)			
a / Å	8.6867(4)	8.6742(3)	8.6615(4)	8.6502(3)
c / Å	25.3813(15)	25.3428(10)	25.4130(14)	25.3992(11)
V / Å^3	1915.24(17)	1906.84(12)	1906.52(16)	1900.52(12)
Z	2			
ρ_{calc} / g cm^{-3}	2.1851	2.1968	2.1986	2.2113
μ / mm^{-1}	8.857	8.970	9.055	9.168
F_{000}	1200	1202	1204	1206
Crystal size / mm^3	0.030 × 0.030 × 0.010	0.060 × 0.060 × 0.015	0.10 × 0.10 × 0.050	0.12 × 0.12 × 0.060
Radiation	Mo Kα (λ = 0.71073 Å)			
2θ range / °	4.68-52.74	4.70-53.46	4.70-56.54	4.70-56.64
Reflec collected	23389	26029	29993	31013
Indep reflections	1018	1050	1227	1226
R_{int}, R_σ	0.0838, 0.0214	0.0532, 0.0137	0.0364, 0.0110	0.0335, 0.0101
Parameters/restraints	91/3	91/3	91/3	91/3
S (on F^2)	1.111	1.115	1.080	1.032
R_1, wR_2 ($I \geq 2\sigma(I)$)	0.0287, 0.0489	0.0175, 0.0321	0.0150, 0.0303	0.0166, 0.0603
R_1, wR_2 (all data)	0.0466, 0.0537	0.0300, 0.0362	0.0231, 0.0329	0.0234, 0.0671
$\Delta\rho_{max}/\Delta\rho_{min}$ / e Å^{-3}	1.27/–1.49	0.95/–0.95	1.38/–0.60	2.01/–0.66

Table S2. Crystallographic data and refinement parameters for **1Ln** (**Ln = Sm, Eu, Tb, Dy**).

	1Sm	**1Eu**	**1Tb**	**1Dy**
Formula	$C_{24}H_{44}NO_8Pt_2S_8Sm$	$C_{24}H_{44}EuNO_8Pt_2S_8$	$C_{24}H_{44}NO_8Pt_2S_8Tb$	$C_{24}H_{44}DyNO_8Pt_2S_8$
M_r	1271.67	1273.27	1280.23	1283.80
T / K	122(1)			
Crystal system	Tetragonal			
Space group	*P*4/*mcc* (No. 124)			
a / Å	8.6302(3)	8.6247(3)	8.6049(3)	8.6098(11)
c / Å	25.4187(9)	25.4329(9)	25.4824(11)	25.515(4)
V / Å^3	1893.19(11)	1891.84(11)	1886.83(12)	1891.4(5)
Z	2			
ρ_{calc} / g cm^{-3}	2.2306	2.2350	2.2532	2.2541
μ / mm^{-1}	9.383	9.49	9.733	9.815
F_{000}	1210	1212	1216	1218
Crystal size / mm^3	0.12 × 0.12 × 0.040	0.17 × 0.17 × 0.030	0.040 × 0.040 × 0.010	0.080 × 0.080 × 0.020
Radiation	Mo Kα (λ = 0.71073 Å)			
2θ range / °	4.71-56.56	4.72-56.54	4.74-53.46	4.74-56.52
Reflec collected	28103	28473	27238	22513
Indep reflections	1221	1219	1042	1218
R_{int}, R_σ	0.364, 0.0114	0.0362, 0.0113	0.0597, 0.0155	0.0584, 0.0239
Parameters/restraints	91/3	91/3	91/3	91/3
S (on F^2)	1.090	1.114	1.086	1.073
R_1, wR_2 ($I \geq 2\sigma(I)$)	0.0140, 0.0292	0.0165, 0.0339	0.0177, 0.0347	0.0182, 0.0374
R_1, wR_2 (all data)	0.0213, 0.0321	0.0232, 0.362	0.0298, 0.0390	0.0283, 0.0409
$\Delta\rho_{max}/\Delta\rho_{min}$ / e Å^{-3}	1.37/–1.59	0.78/–0.70	1.13/–0.90	0.88/–0.93

Table S3. Crystallographic data and refinement parameters for **1Ln** (**Ln = Ho – Yb**).

	1Ho	**1Er**	**1Tm**	**1Yb**
Formula	$C_{24}H_{44}HoNO_8Pt_2S_8$	$C_{24}H_{44}ErNO_8Pt_2S_8$	$C_{24}H_{44}NO_8Pt_2S_8Tm$	$C_{24}H_{44}NO_8Pt_2S_8Yb$
M_r	1286.23	1288.56	1290.24	1294.34
T / K	122(1)			
Crystal system	Tetragonal			
Space group	*P*4/*mcc* (No. 124)			
a / Å	8.5991(3)	8.5857(3)	8.5844(4)	8.5693(4)
c / Å	25.4691(9)	25.5107(9)	25.5043(14)	25.5201(14)
V / Å^3	1883.32(11)	1880.50(11)	1879.46(16)	1874.02(16)
Z	2			
ρ_{calc} / g cm^{-3}	2.2680	2.2755	2.2797	2.2937
μ / mm^{-1}	9.974	10.116	10.250	10.408
F_{000}	1220	1222	1224	1226
Crystal size / mm^3	0.10 × 0.10 × 0.030	0.11 × 0.11 × 0.050	0.060 × 0.060 × 0.015	0.090 × 0.090 × 0.025
Radiation	Mo Kα (λ = 0.71073 Å)			
2θ range / °	4.84-55.76	4.74-56.54	4.74-56.56	4.76-56.56
Reflec collected	28578	31009	34470	30283
Indep reflections	1164	1213	1213	1211
R_{int}, R_σ	0.0475, 0.0147	0.0375, 0.0112	0.0597, 0.0164	0.0392, 0.0121
Parameters/restraints	91/3	91/3	91/3	91/3
S (on F^2)	1.102	1.097	1.096	1.065
R_1, wR_2 ($I \geq 2\sigma(I)$)	0.0170, 0.0284	0.0140, 0.0295	0.0189, 0.0336	0.0145, 0.0296
R_1, wR_2 (all data)	0.0262, 0.0306	0.0219, 0.0322	0.0325, 0.0374	0.0217, 0.0330
$\Delta\rho_{max}/\Delta\rho_{min}$ / e Å^{-3}	0.97/–1.13	1.31/–0.76	1.23 /–1.21	2.51/–1.23

Table S4. Crystallographic data and refinement parameters for **1Ln** (**Ln = Lu, Y**) at 122 K and **1Gd** at RT.

	1Lu	**1Y**	**1Gd @ RT**
Formula	$C_{24}H_{44}LuNO_8Pt_2S_8$	$C_{24}H_{44}NO_8Pt_2S_8Y$	$C_{24}H_{44}GdNO_8Pt_2S_8$
M_r	1296.27	1210.23	1278.56
T / K	122(1)		295(1)
Crystal system	Tetragonal		Tetragonal
Space group	*P*4/*mcc* (No. 124)		*P*4/*mcc* (No. 124)
a / Å	8.5697(3)	8.5854(4)	8.8600(4)
c / Å	25.5067(10)	25.5257(15)	25.8359(12)
V / Å^3	1873.21(12)	1881.48(17)	1946.54(16)
Z	2		2
ρ_{calc} / g cm^{-3}	2.2981	2.1361	2.1813
μ / mm^{-1}	10.551	9.448	9.321
F_{000}	1228	1164	1214
Crystal size / mm^3	0.090 × 0.090 × 0.030	0.11 × 0.11 × 0.030	0.10 × 0.10 × 0.030
Radiation	Mo Kα (λ = 0.71073 Å)		Mo Kα (λ = 0.71073 Å)
2θ range / °	4.76-55.70	4.74-56.52	4.70-55.68
Reflec collected	34697	29876	28211
Indep reflections	1158	1213	1205
R_{int}, R_σ	0.0395, 0.0104	0.0435, 0.0136	0.0443, 0.0142
Parameters/restraints	91/3	91/3	91/3
S (on F^2)	1.117	1.059	1.042
R_1, wR_2 ($I \geq 2\sigma(I)$)	0.0172, 0.0365	0.0143, 0.0296	0.0210, 0.0653
R_1, wR_2 (all data)	0.0243, 0.0396	0.0225, 0.0327	0.0316, 0.0740
$\Delta\rho_{max}/\Delta\rho_{min}$ / e Å^{-3}	1.38/–0.73	1.56/–0.63	0.89/–1.22

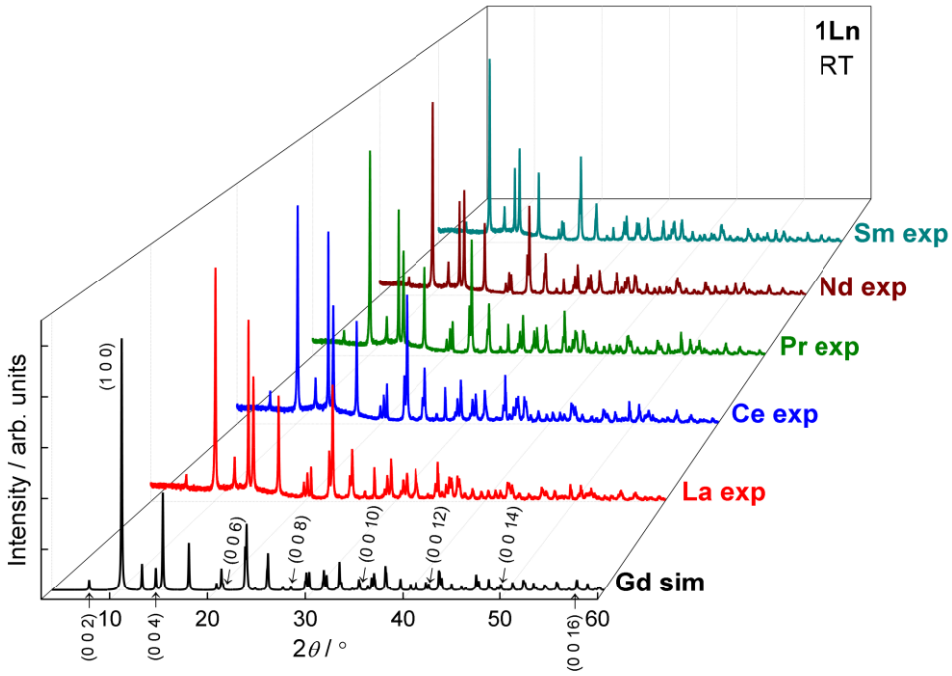

Figure S1. Room temperature PXRD patterns of **1Ln** (**Ln = La – Nd, Sm**) compared to the pattern of **1Gd** simulated from the room temperature structure. In the latter powder pattern, the indices of the peaks relevant for the discussion of orientation effects are given.

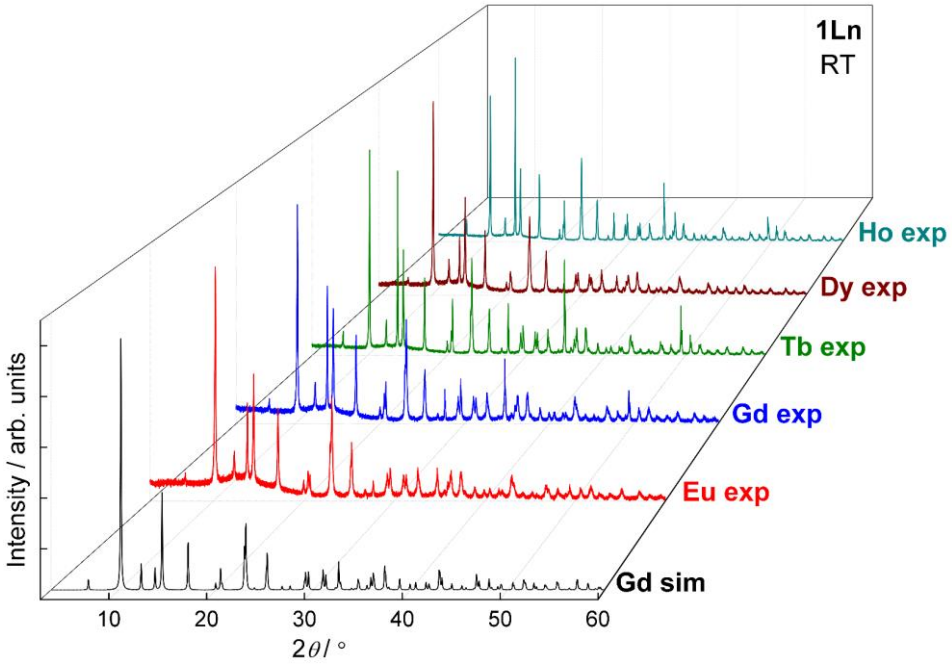

Figure S2. Room temperature PXRD patterns of **1Ln** (**Ln = Eu – Ho**) compared to the pattern of **1Gd** simulated from the room temperature structure.

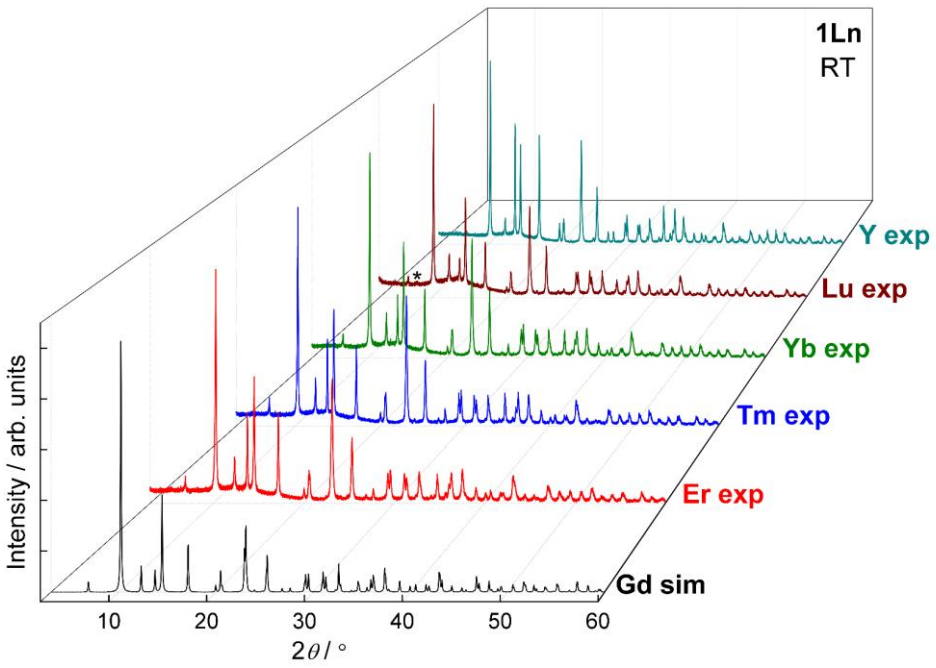

Figure S3. Room temperature PXRD patterns of **1Ln** (**Ln = Er – Lu, Y**) compared to the pattern of **1Gd** simulated from the room temperature structure. The asterisk above the pattern of **1Lu** marks a Bragg peak belonging to a minor crystalline impurity.

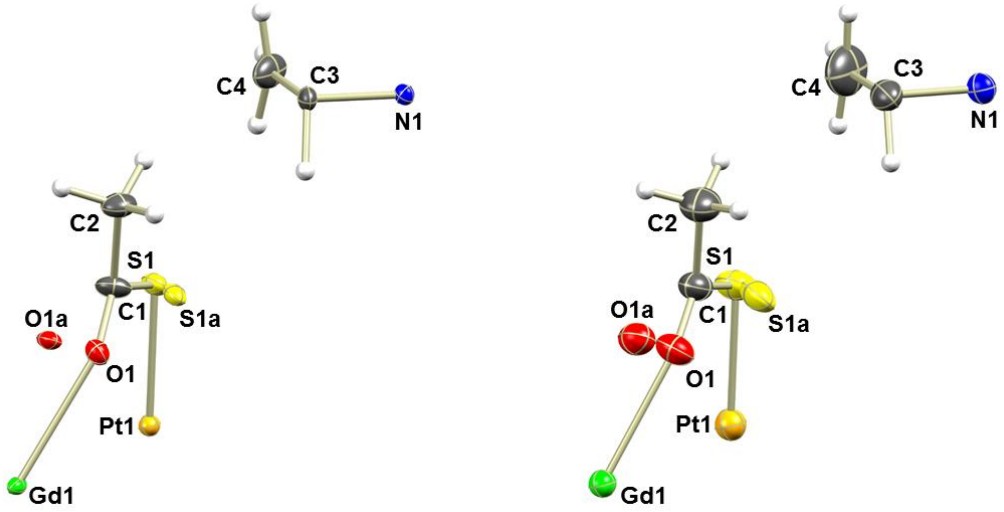

Figure S4. Thermal ellipsoids plots (50 % probability) of the asymmetric units of **1Gd** at 122 K (*left*) and at RT (*right*) with atomic labels. Colour code: Gd, green; Pt, orange; S, yellow; O, red; N, blue; C, dark grey; H, light grey.

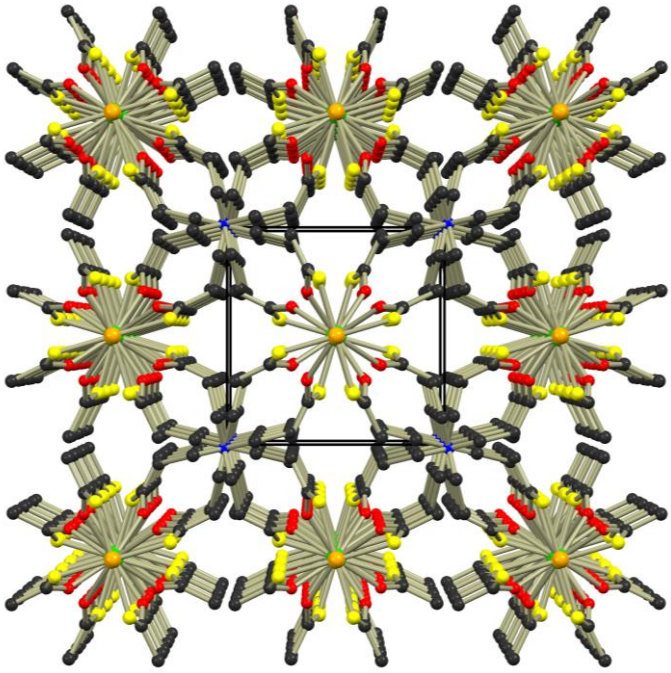

Figure S5. Perspective view along the *c*-axis of the crystal packing for **1Gd**. The black lines outline the *a*- and *b*-axes of the unit cell. Hydrogen atoms have been omitted for clarity. Likewise, only one of the two disordered fragments is shown. Colour code: Gd, green; Pt, orange; S, yellow; O, red; N, blue; C, dark grey.

Discussion of the unit cell parameters for 1Ln

The unit cell parameters at T = 122(1) K for the **1Ln** compounds obtained from single crystal X-ray diffraction experiments are summarized in Fig. 4. The length of the *a*-axis (and consequently also the *b*-axis) decreases from 8.6867(4) Å for the **1La** to 8.5697(3) Å for **1Lu**, in accordance with the expected trend resulting from the lanthanide contraction. Surprisingly, the opposite trend is found for the length of the *c*-axis of the unit cell; this length slightly increases across the *f*-block. The unexpected result can be understood by examining the trend in θ (Fig. 3). As the ionic radii of the lanthanide ions decrease, the shortest distance between oxygen atoms belonging to different metalloligands would be expected to do so as well. However, a decrease in θ circumvents this electrostatically unfavourable scenario. Indeed, the shortest inter-metalloligand oxygen-oxygen distance is roughly independent of the lanthanide (**1La**: O1–O1 = 2.644(15) Å, O1a–O1a = 2.343(15) Å, **1Lu**: O1–O1 = 2.606(10) Å, O1a–O1a = 2.387(10) Å). Upon the decrease in axial compression, the intramolecular Pt···Pt distance increases from 7.3246(10) Å in **1La** to 7.4338(5) Å in **1Lu**. In this light, the slight expansion along the *c*-axis, can counterintuitively be taken as a result of the lanthanide contraction. The contractions along the *a*- and *b*-axes are greater than the expansion along the *c*-axis (1.4 % vs. 0.9 %), and consequently the expected decrease in unit cell volume upon traversing the *f*-block is observed.

Table S5. Crystallographic data and refinement parameters for **2Ln** (**Ln = Tb – Ho**).

	2Tb	**2Dy**	**2Ho**
Formula	$C_{40}H_{44}O_8PPt_2S_8Tb$	$C_{40}H_{44}DyO_8PPt_2S_8$	$C_{40}H_{44}HoO_8PPt_2S_8$
M_r	1489.37	1492.95	1495.38
T / K		123(1)	
Crystal system		Tetragonal	
Space group		*P*4/*n* (No. 85)	
a / Å	12.6486(6)	12.6485(7)	12.6459(4)
c / Å	15.1552(10)	15.1509(8)	15.1400(5)
V / Å^3	2423.9(2)	2423.9(2)	2421.17(13)
Z		2	
ρ_{calc} / g cm^{-3}	2.0399	2.0454	2.0510
μ / mm^{-1}	7.622	7.706	7.806
F_{000}	1424	1426	1428
Crystal size / mm^3	0.075 × 0.075 × 0.030	0.075 × 0.075 × 0.025	0.080 × 0.080 × 0.050
Radiation		Mo Kα (λ = 0.71073 Å)	
2θ range / °	5.28-57.38	4.56-52.46	4.56-57.40
Reflec collected	52845	28695	46482
Indep reflections	3146	2584	3145
R_{int}, R_σ	0.0706, 0.0270	0.0936, 0.0371	0.0534, 0.0215
Parameters/restraints	139/0	139/0	139/0
S (on F^2)	1.049	1.007	1.034
R_1, wR_2 ($I \geq 2\sigma(I)$)	0.0224, 0.0354	0.0245, 0.0357	0.0201, 0.0371
R_1, wR_2 (all data)	0.0380, 0.0388	0.0478, 0.0405	0.0320, 0.0403
$\Delta\rho_{max}/\Delta\rho_{min}$ / e Å^{-3}	1.99/–1.27	1.38/–1.52	2.13/–0.98

Table S6. Crystallographic data and refinement parameters for **2Ln** (**Ln = Er, Y**) at 123 K and **2Gd** at RT.

	2Er	**2Y**	**2Gd @ RT**
Formula	$C_{40}H_{44}ErO_8PPt_2S_8$	$C_{40}H_{44}O_8PPt_2S_8Y$	$C_{24}H_{44}GdO_8PPt_2S_8$
M_r	1497.70	1419.27	1487.70
T / K	123(1)		295(1)
Crystal system	Tetragonal		Tetragonal
Space group	*P*4/*n* (No. 85)		*P*4/*n* (No. 85)
a / Å	12.6367(4)	12.6436(5)	12.800(2)
c / Å	15.1479(6)	15.1616(7)	15.345(3)
V / Å^3	2418.91(14)	2423.74(18)	2514.2(8)
Z	2		2
ρ_{calc} / g cm^{-3}	2.0562	1.9447	1.9650
μ / mm^{-1}	7.912	7.382	7.262
F_{000}	1430	1372	1422
Crystal size / mm^3	0.10 × 0.10 × 0.030	0.125 × 0.125 × 0.030	0.10 × 0.10 × 0.030
Radiation	Mo Kα (λ = 0.71073 Å)		Mo Kα (λ = 0.71073 Å)
2θ range / °	4.56-57.38	4.56-56.56	5.22-53.46
Reflec collected	45171	44184	37300
Indep reflections	3142	3020	2678
R_{int}, R_σ	0.0573, 0.0238	0.0504, 0.0199	0.0640, 0.0253
Parameters/restraints	139/0	139/0	139/0
S (on F^2)	1.038	1.038	1.051
R_1, wR_2 ($I \geq 2\sigma(I)$)	0.0207, 0.0373	0.0176, 0.0344	0.0254, 0.0581
R_1, wR_2 (all data)	0.0333, 0.0407	0.0242, 0.0363	0.0370, 0.0640
$\Delta\rho_{max}/\Delta\rho_{min}$ / e Å^{-3}	2.90/–1.77	1.11/–0.67	1.66/–0.79

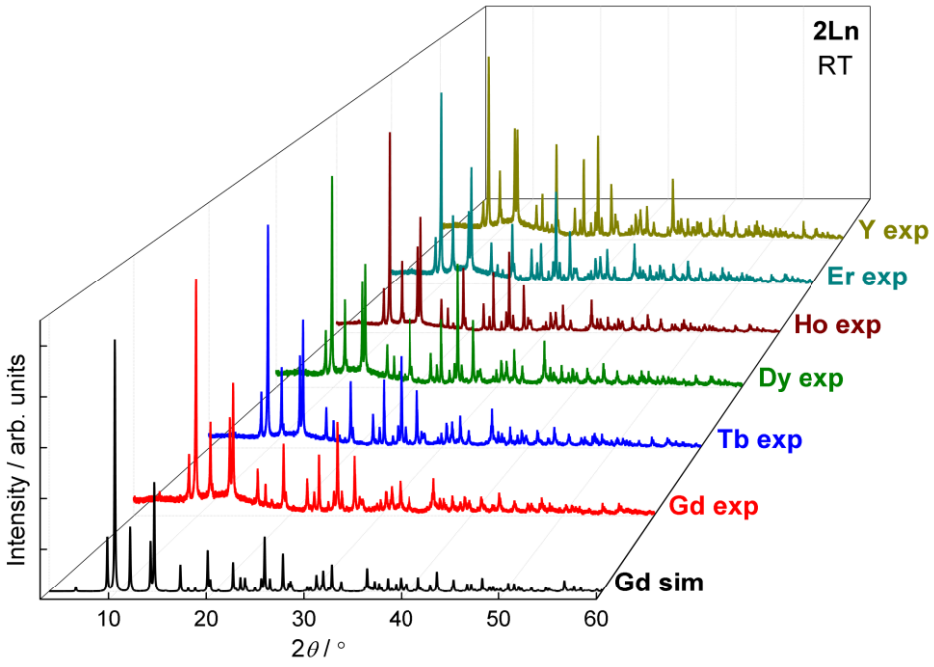

Figure S6. Room temperature PXRD patterns of **2Ln** compared to the pattern of **2Gd** simulated from the room temperature structure.

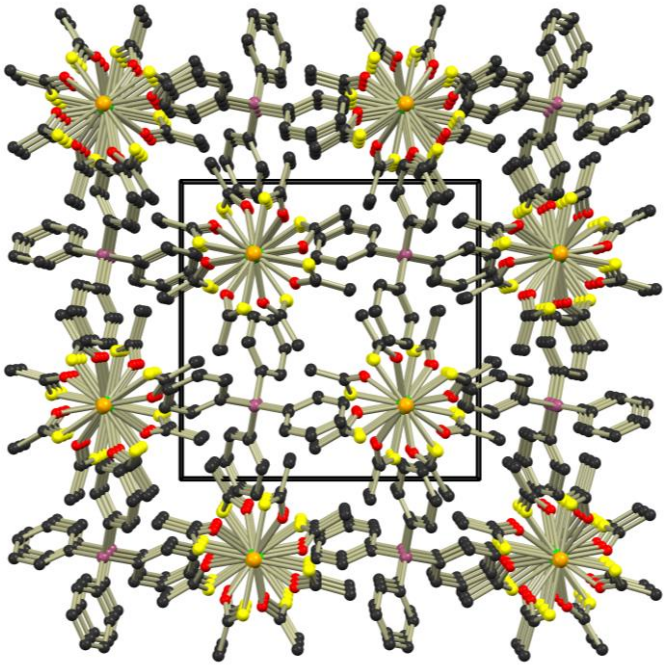

Figure S7. Perspective view along the *c*-axis of the crystal packing for **2Gd**. The black lines outline the *a*- and *b*-axes of the unit cell. Hydrogen atoms have been omitted for clarity. Colour code: Gd, green; Pt, orange; S, yellow; O, red; P, purple; C, dark grey.

Table S7. Crystallographic data and refinement parameters for **1Ln′** (**Ln = Y, Gd**), and **2Ln′** (**Ln = Y, Gd**).

	1Y′	**1Gd′**	**2Y′**	**2Gd′**
Formula	$C_{24}H_{44}NO_8Pd_2S_8Y$	$C_{24}H_{44}GdNO_8Pd_2S_8$	$C_{40}H_{44}O_8PPd_2S_8Y$	$C_{40}H_{44}GdO_8PPd_2S_8$
M_r	1032.79	1101.23	1241.91	1310.38
T / K	295(1)		295(1)	
Crystal system	Tetragonal		Tetragonal	
Space group	*P*4/*mcc* (No. 124)		*P*4/*n* (No. 85)	
a / Å	8.6638(3)	8.6832(2)	12.8004(5)	12.8122(7)
c / Å	25.8747(9)	25.8856(9)	15.3730(6)	15.3823(7)
V / Å^3	1942.19(12)	1951.72(9)	2518.87(17)	2525.0(2)
Z	2		2	
ρ_{calc} / g cm^{-3}	1.7661	1.8737	1.6375	1.7234
μ / mm^{-1}	2.886	3.060	2.271	2.411
F_{000}	1036	1086	1244	1294
Crystal size / mm^3	0.13 × 0.13 × 0.030	0.13 × 0.13 × 0.030	0.195 × 0.195 × 0.14	0.195 × 0.195 × 0.14
Radiation	Mo Kα (λ = 0.71073 Å)		Mo Kα (λ = 0.71073 Å)	
2θ range / °	4.7-57.38	4.7-54.94	4.5-56.56	4.5-55.74
Reflec collected	16013	32169	30667	22499
Indep reflections	1296	1160	3142	3023
R_{int}, R_σ	0.0386, 0.0187	0.0781, 0.0207	0.0370, 0.0203	0.0409, 0.0268
Parameters/restraints	91/3	91/3	139/0	139/0
S (on F^2)	1.088	1.102	1.028	1.020
R_1, wR_2 ($I \geq 2\sigma(I)$)	0.0246, 0.0467	0.0283, 0.0480	0.0490, 0.1287	0.0399, 0.0914
R_1, wR_2 (all data)	0.0378, 0.0514	0.0480, 0.0533	0.0667, 0.1424	0.0577, 0.1006
$\Delta\rho_{max}/\Delta\rho_{min}$ / e Å^{-3}	0.49/–0.59	0.76/–0.99	2.21/–1.25	1.87/–1.19

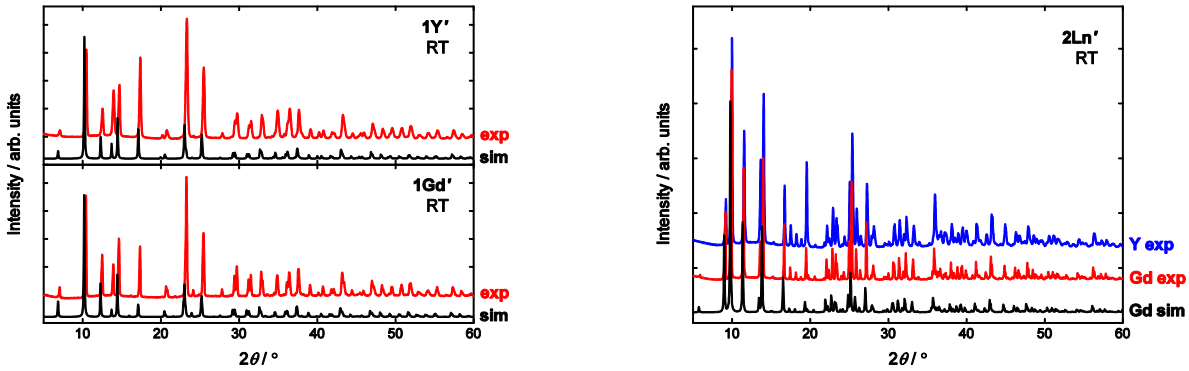

Figure S8. Room temperature PXRD patterns of **1Gd′** and **1Y′** along with those simulated based on the room temperature structures (*left*), and the PXRD patterns of **2Gd′** and **2Y′** along with the simulated pattern of **2Gd′** based on the room temperature structure (*right*).

Magnetic measurements

Magnetic measurements were carried out on a Quantum Design MPMS-XL SQUID magnetometer equipped with a 5 T dc magnet. The dc susceptibility measurements were conducted in an applied field of B = 100 mT. For all measurements, the crystalline samples were ground into fine powders using an agate mortar. Between 20 and 30 mg of powder was loaded into a polycarbonate capsule, gently compressed by hand using the end of a small glass rod, and covered in hexadecane to avoid field-induced orientation of the crystallites. Due to the melting point of hexadecane (mp = 291 K), the samples were always inserted in the magnetometer at T = 10 K in zero applied dc field, and the sample was never heated above 280 K. The data work-up was carried out using the MagProp utility of the Data Analysis and Visualization Environment program package DAVE.[6] All data were corrected for diamagnetism of the sample by means of Pascal's constants,[7] and of the polycarbonate capsule and hexadecane ($\chi = -5 \cdot 10^{-7}$ cm^3 g^{-1}). The magnetic susceptibility was calculated as $\chi = M/B$.

Table S8. High-temperature values of the molar magnetic susceptibility-temperature product compared to the expected Curie constants for the various trivalent lanthanide ions.

Ln	$\chi T_{T = 280\ \mathrm{K}}$(**1Ln**) / cm^3 mol^{-1} K	$\chi T_{T = 280\ \mathrm{K}}$(**2Ln**) / cm^3 mol^{-1} K	C / cm^3 mol^{-1} K
Gd	7.74	8.11	7.88
Tb	11.83	11.86	11.82
Dy	14.07	14.17	14.17
Ho	13.89	13.92	14.07
Er	11.26	11.60	11.48
Tm	6.95	N/A	7.15
Yb	2.53	N/A	2.57

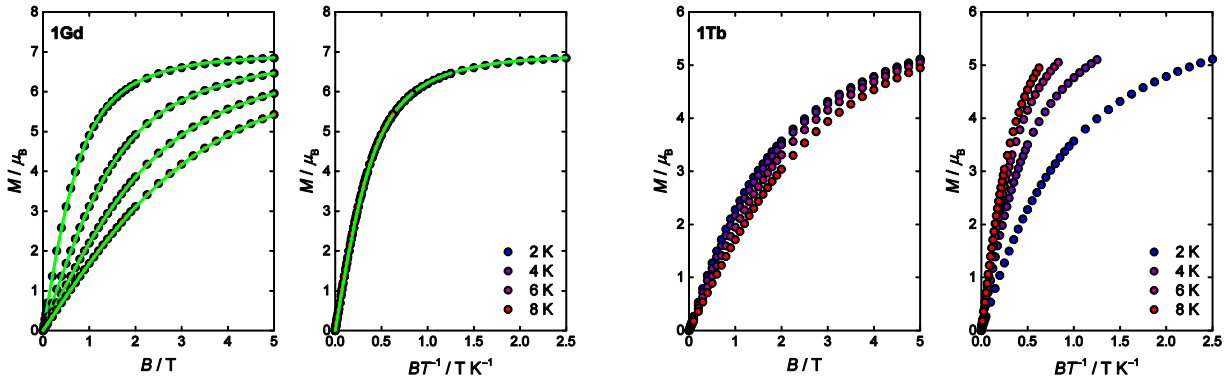

Figure S9. Plots of *M* vs. *B* and reduced magnetization isotherms for **1Gd** and **1Tb**. The green lines represent a collective fit of the $\chi T(T)$ and reduced magnetization data for **1Gd** to an isotropic Zeeman Hamiltonian yielding g_{iso} = 1.98(3).

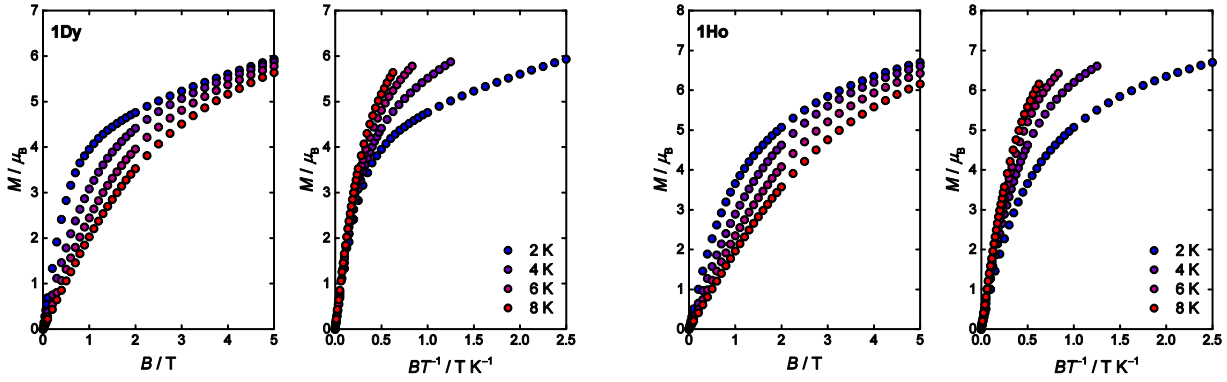

Figure S10. Plots of *M* vs. *B* and reduced magnetization isotherms for **1Dy** and **1Ho**.

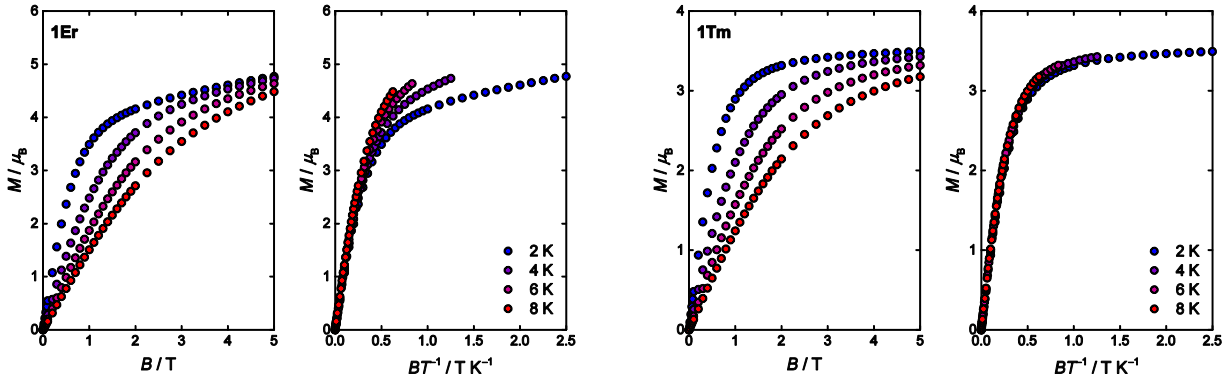

Figure S11. Plots of *M* vs. *B* and reduced magnetization isotherms for **1Er** and **1Tm**.

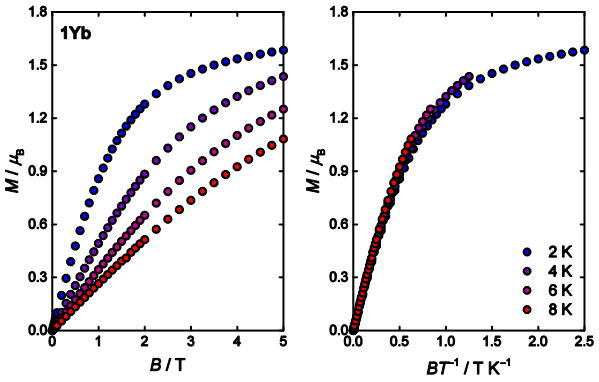

Figure S12. Plots of *M* vs. *B* and reduced magnetization isotherms for **1Yb**.

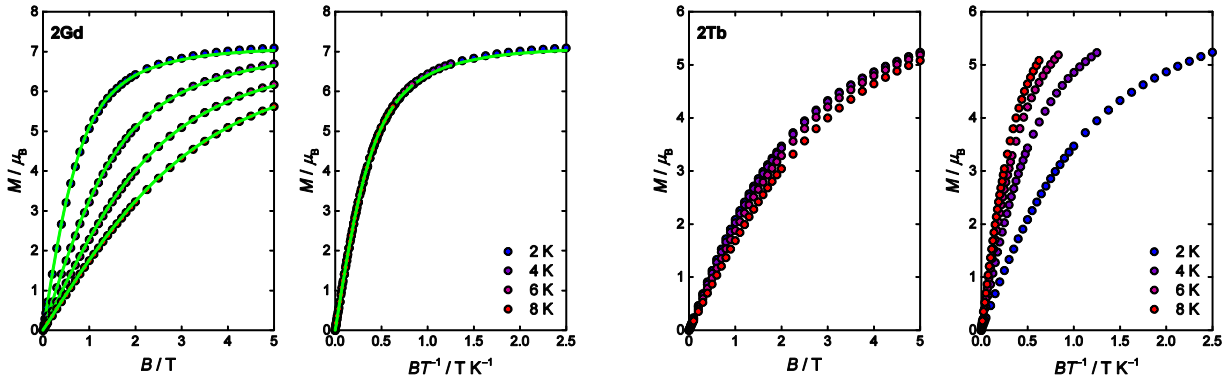

Figure S13. Plots of *M* vs. *B* and reduced magnetization isotherms for **2Gd** and **2Tb**. The green lines represent a collective fit of the $\chi T(T)$ and reduced magnetization data for **2Gd** to an isotropic Zeeman Hamiltonian yielding g_{iso} = 2.03(3).

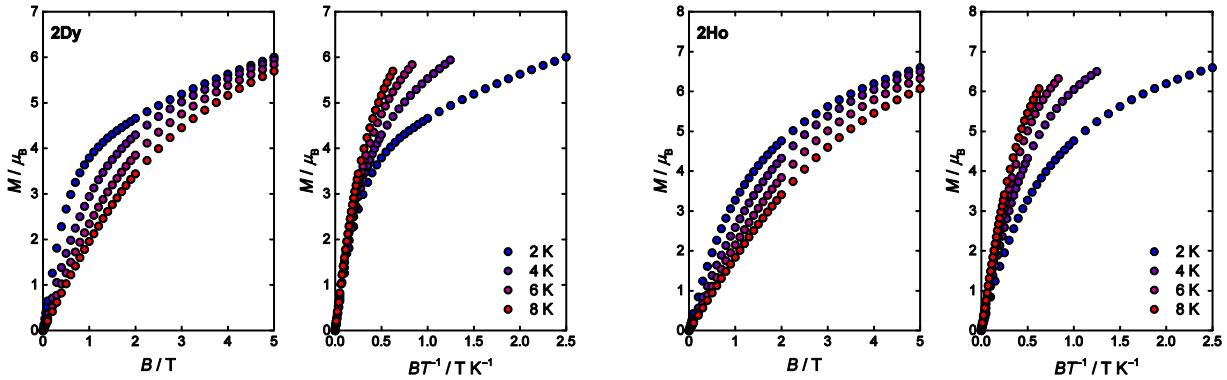

Figure S14. Plots of *M* vs. *B* and reduced magnetization isotherms for **2Dy** and **2Ho**.

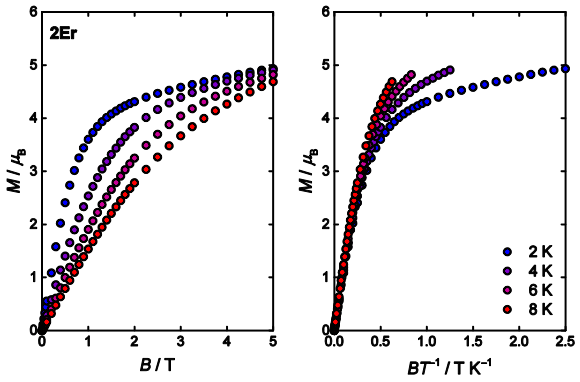

Figure S15. Plots of *M* vs. *B* and reduced magnetization isotherms for **2Er**.

EPR spectroscopy

Room temperature powder and single-crystal X-band EPR spectra were acquired on Bruker E500 EPR instrument equipped with an X-band bridge. For the powder measurements, the samples were thoroughly ground in agate mortar and measured in a quartz tube. Single crystals were mounted on an acrylic rod that was held in a quartz tube similar to that used for powder measurements. The single crystals were rotated in steps of 2° using a computer-controlled goniometer. The diluted samples **1Y$_{0.98}$Gd$_{0.02}$** and **1Y$_{0.98}$Gd$_{0.02}$′** were prepared employing the procedure for **1Y** and **1Y′**, respectively using $YCl_3 \cdot 6H_2O$ and $GdCl_3 \cdot 6H_2O$ in a 49:1 molar ratio. The **2Y$_{0.98}$Gd$_{0.02}$** and **2Y$_{0.98}$Gd$_{0.02}$′** samples were prepared according to the general procedure for **2Ln** and **2Ln′** employing crude $[N^nPr_4][Y\{M(SAc)_4\}_2]$ and $[N^nPr_4][Gd\{M(SAc)_4\}_2]$ (**2Ln**, M = Pt; **2Ln′**, M = Pd) in a 49:1 molar ratio. A suitable single crystal of **2Y$_{0.98}$Gd$_{0.02}$** was grown by recrystallizing the product from the **2Ln** procedure in boiling $MeNO_2$ (25 mg in 7 ml), while the single crystal of **1Y$_{0.98}$Gd$_{0.02}$** was obtained directly from the reaction mixture.

Single crystals of **1Y$_{0.98}$Gd$_{0.02}$** and **2Y$_{0.98}$Gd$_{0.02}$** were rotated around an axis close to the crystallographic *c* axis with, consequently, the magnetic field being in the *ab* plane, as well as rotated around an axis contained in the *ab* plane thereby rotating the magnetic field in a plane containing the *c* axis. Each line position $B_{ij,\mathrm{exp}}$, where *ij* is an appropriate assignment of the line as a resonance involving energy levels *i* and *j*, was used in the minimization of

$$\chi^2 = \frac{\sum (B_{ij,\mathrm{exp}} - B_{ij,\mathrm{mod}})^2}{\sigma^2} \tag{S1}$$

with $B_{ij,\mathrm{mod}}$ being the calculated resonance magnetic field corresponding to $B_{ij,\mathrm{exp}}$ based on the effective spin Hamiltonian model

$$\hat{H} = \sum_{k=2,4,6} \sum_{q=-k}^{k} P_k^q U_k^q + \mu_\mathrm{B}(g_x S_x B_x + g_y S_y B_y + g_z S_z B_z) \tag{S2}$$

where $g_x = g_y = g_\perp$ and $g_z = g_\parallel$, and the U_k^q operator is defined by having the following matrix elements

$$\langle SM | U_k^q | SM' \rangle = (-1)^{S-M} \begin{pmatrix} S & k & S \\ -M & q & M \end{pmatrix} \tag{S3}$$

i.e. the usual Wigner-Eckart theorem with the reduced matrix element set to unity.

As a result of imperfect mount of a small crystal on an imperfect support there is some uncertainty in the precise dispositioning of the crystal in the cavity. Therefore, we initially allowed all parameters P_k^q to be free parameters in the minimization of eq. S1. As expected, this resulted in some parameters having estimated standard deviations much larger than their value. These were subsequently omitted in the treatment. The magnitude of the inherent uncertainty in the crystal position was checked by using the estimated P'^q_2 parameters as follows. The parameter vector (P'^{-2}_2, P'^{-1}_2, P'^0_2, P'^1_2, P'^2_2) was subjected to a Wigner rotation (P'^{-2}_2, P'^{-1}_2, P'^0_2, P'^1_2, P'^2_2)$D^{(2)}(\alpha,\beta,\gamma)$ = (P^{-2}_2, P^{-1}_2, P^0_2, P^1_2, P^2_2), where β,γ were determined so as to minimize $(P^{-2}_2)^2 + (P^{-1}_2)^2 + (P^1_2)^2 + (P^2_2)^2$. In all cases the β,γ values indicated a misagreement of at most 3 degrees between the intended and the actual rotation axis.

The software for the fittings was developed in house and has previously been described.[8] In order to translate the determined P_k^q parameters into B_k^q parameters, corresponding to the typical Stevens operator definitions, the following conversion was applied

$$B_k^q = \frac{P_k^q}{\langle S||O_k||S\rangle}, \qquad \langle S||O_k||S\rangle = \frac{1}{2^k}\sqrt{\frac{(2S+k+1)!}{(2S-k)!}} \tag{S4}$$

with S = 7/2.

References

1 *Bruker; Bruker AXS Inc. SAINT, Version 7.68A; Bruker AXS: Madison, WI, 2009.*

2 G. Sheldrick, *SADABS, Version 2008/2; University of Göttingen: Germany, 2003.*

3 O. V. Dolomanov, L. J. Bourhis, R. J. Gildea, J. A. K. Howard and H. Puschmann, *J. Appl. Crystallogr.*, 2009, **42**, 339–341.

4 L. J. Bourhis, O. V. Dolomanov, R. J. Gildea, J. A. K. Howard and H. Puschmann, *Acta Crystallogr. Sect. A*, 2015, **71**, 59–75.

5 C. F. Macrae, P. R. Edgington, P. McCabe, E. Pidcock, G. P. Shields, R. Taylor, M. Towler and J. van de Streek, *J. Appl. Crystallogr.*, 2006, **39**, 453–457.

6 R. T. Azuah, L. R. Kneller, Y. Qiu, P. L. W. Tregenna-Piggott, C. M. Brown, J. R. D. Copley and R. M. Dimeo, *J. Res. Natl. Inst. Stand. Technol.*, 2009, **114**, 341-358.

7 G. A. Bain and J. F. Berry, *J. Chem. Educ.*, 2008, **85**, 532–536.

8 H. H. Mor, J. Bendix and H. Weihe. *J. Mag. Res*. 2010, **207**, 283-286.